Palaeogeography, Palaeoclimatology, Palaeoecology 414 (2014) 486–492

Contents lists available at ScienceDirect

Palaeogeography, Palaeoclimatology, Palaeoecology

journal homepage: www.elsevier.com/locate/palaeo

On porosity of archeological bones I — Textural characterization of pathological Spanish medieval human bones

Pedro Bosch [a,*], Carlos Moreno-Castilla [b], Zulamita Zapata-Benabithe [b], Inmaculada Alemán [c], Victor Hugo Lara [d], Josefina Mansilla [e], Carmen Pijoan [e], Miguel Botella [c]

[a] Instituto de Investigaciones en Materiales, Universidad Nacional Autónoma de México, 0451 México D.F., Mexico
[b] Departamento de Química Inorgánica, Facultad de Ciencias, Universidad de Granada, 18002 Granada, Spain
[c] Laboratorio de Antropología, Facultad de Medicina, Universidad de Granada, 18012 Granada, Spain
[d] Universidad Autónoma Metropolitana — Iztapalapa, Avenida San Rafael Atlixco 186, 09340 México D.F., Mexico
[e] Dirección de Antropología Física, Instituto Nacional de Antropología e Historia, Gandhi s/n, Polanco, 11560 México D.F., Mexico

ARTICLE INFO

Article history:
Received 31 March 2014
Accepted 18 September 2014
Available online 2 October 2014

Keywords:
Gas adsorption
small angle X-ray Scattering
Texture
Porosity
Poblet
Granada

ABSTRACT

Bone texture may vary as a function of age, pathology as well as on bone treatments; thus absolute values of specific surface area or porosity are not often reported. A review of the anthropological and archeological references reveals that the results obtained with the current methodologies for the textural analysis of bone may be contradictory. Indeed, the characterization of archeological bone is a very difficult task through conventional techniques. Still, it is most relevant as porosity is the symptom of several pathologies, for instance anemia, osteoporosis, hyperostosis or syphilis.

In this work, archeological bone samples – pathological or healthy – were characterized by nitrogen adsorption–desorption isotherms at −196 °C, small angle X-ray scattering (SAXS) and scanning electron microscopy (SEM). The studied bones are healthy, osteoporotic, hyperostosic, and syphilitic. Porosity, specific surface area, and morphology as well as non conventional features such as roughness, specific surface or fractal dimension, are correlated with the well known macroscopical reported symptoms. The samples come from Moorish Andalucía (Grenade) and Medieval Catalonia (Poblet Monastery).

1. Introduction

Bone is constituted by connective tissue composed of an organic protein, collagen, and a mineral component, hydroxyapatite (Weiner and Traub, 1992; Labastida Pólito et al., 2006). Collagen appears in bone as beams of white inelastic fibers with an enormous tensile strength. Those fibers include fibrils, which are formed by smaller filaments: the collagen protein that is the most abundant protein in animal tissues. Human collagen protein contains a high percentage (23 to 30%) of proline and hydroxyproline amino acids. The end space of the collagen fibrils is the nucleation center for calcium phosphate, *i.e.*, hydroxyapatite. Depending on collagen fiber orientation, two types of bone are distinguished: cortical which appears in long bones or trabecular that may be found in vertebrae or extremities of long bones. Note that lamellar bone is not restricted to cortical, but refers to the organization of the collagen fibers. Normal adult human trabecular bone is lamellar as well.

Human bones have three main cavities: Harvesian canals (50 μm), osteocytic voids (quasi ellipsoidal and a few μm in size) and canaliculi (found between the lacunae, their diameter is less than one μm). Still, there are other cavities in bone besides these, *e.g.*, the canals of forming osteons, and resorptive bays which are much larger, and vascular canals. The cortical porosity increases from approximately 8% for young individuals up to 24–28% for elderly individuals. Harvesian canals increase significantly with age whereas lacuna porosity decreases slightly (Martin, 1984; Wang and Ni, 2003). There are pathologies such as anemia (Domínguez-Rodrigo et al., 2012), syphilis (Lopes et al., 2010), leprosy (Roffey and Tucker, 2012), or co-deficiency of vitamin C and B_{12} (Walker et al., 2009) well known for their impact on bone porosity. Furthermore, bone pores may be modified, also, by *postmortem* thermal treatments (Bosch et al., 2011).

In this work, we have chosen to study and compare bones which at first glance, *i.e.* by macroscopical criteria, are altered in their porosity at various degrees (Ortner, 2011). They correspond to Moorish Andalucía and Medieval Catalonia, in Spain. As bone evolves with age and pathology as well as with bone treatments, the characterization of bone texture is hard work, and no absolute values of specific surface area or porosity are acceptable.

A review of the anthropological and archeological references reveals that the results obtained with the current methodologies for the textural analysis of bone are often contradictory. It is difficult to understand

* Corresponding author. Tel.: +52 56 22 46 56.
E-mail address: croqcroq@hotmail.com (P. Bosch).

http://dx.doi.org/10.1016/j.palaeo.2014.09.018
0031-0182/

measurements as they depend not only on bone condition (taphonomy, diagenesis or washing) but also on characterization methods, which *see* different features. Although experiments with SAXS (Hiller and Wess, 2006; Pijoan et al., 2007) or nuclear magnetic resonance, NMR, have been fruitful (Wang and Ni, 2003), the most direct technique to evaluate texture should be gas adsorption as it happens with other materials (Sing, 2001; Fairén-Jiménez et al., 2006; Smith et al., 2008). Indeed, when a gas or vapor phase is brought into contact with a solid, part of it is taken up and remains on the outside attached to the surface, this phenomenon is known as adsorption. In physisorption (*i.e.* physical adsorption), there is a weak attraction (through Van der Waals forces) between the gas and the solid surface. The technique based on those principles is a useful tool to determine specific surface area, pore size distribution, and porosity (Rouquerol et al., 1999).

In this work, results obtained from N_2 adsorption–desorption isotherms at −196 °C are compared to those provided by scanning electron microscopy (SEM) and small angle X-ray scattering (SAXS). The studied materials, mainly tibias (*i.e.* cortical tissue) and skulls (*i.e.* trabecular tissue), are human archeological bones from Spain which present different types of pathology and various degrees of diagenesis. The ultimate purpose is to discuss bone texture and the methods to evaluate it, macro, micro or nano-scopically. The discussion of porosity and cavities is meaningful as the extent of cavities and increased porosity play an important role in the physicochemical dissolution process of calcium phosphates. The larger the exposed surface to the environment, the faster the biomaterial dissolves, simply because larger quantities of exchanges can take place (Barrère et al., 2006).

2. Experimental

2.1. Archeological context

All bones were found in Granada, except for one which comes from the monastery of Poblet. During the Arabic period, in the actual gardens

Fig. 1. Location of Granada and Poblet in Spain.

Table 1
Spanish human bone samples.

Type of bone	Origin (period)$_{classification}$	Labeling	Pathology (macroscopic determination)[a]
Tibia	Poblet (XII–XIIIth century)	SP-tibia-s_1	Syphilis
	Granada (XVth century)$_{TR/05}$	SG-tibia-s_2	Syphilis
	Granada (XIIth century)$_{HR/90}$	SG-tibia-hyp	Hyperostosis
	Granada (XII–XIII century)$_{HR/90}$	SG-tibia-ost	Osteoporosis
	Granada (XI–XIIth century)$_{TR/90}$	SG-tibia-h	Healthy
Skull	Granada (XI–XIIth century)$_{TR/90,\ D\text{-}21/21}$	SG-skull-co	Hyperostosis (criba orbitalia)
	Granada (XVth century)$_{TR/05}$	SG-skull-hyp_1	Hyperostosis
	Granada (XVth century)	SG-skull-hyp_2	Hyperostosis
	Granada (XVth century)$_{Sep\ 243}$	SG-skull-h_1	Healthy
	Granada (XVth century)$_{Sep\ 480}$	SG-skull-h_2	Healthy

[a] Following the criteria of Mays (2008) and Waldron (2009).

of El Triunfo, central Granada was the largest city cemetery, Fig. 1. Founded in the XIth century, it was occupied until the XVIth century. The cemetery was outside the fortified city. In the XXth century it was excavated due to a new urban planning in order to build a parking area. As expected, all corpses were found in lateral *decubitus* position on the right side with the face towards South East.

The bone from the monastery of Poblet corresponds to a different cultural and religious context than the previous ones, although the historical period is the same. Furthermore, the weather and soil composition of Catalonia differ from those of Andalucia; thus, taphonomy should act differently. The Abbey of Santa María de Poblet, founded in 1151, is a Cistercian monastery located in South Catalonia. This monastery was the first of three Cister monasteries, known as the Cistercian triangle, that helped consolidate catholic power in Catalonia in the 12th century, the other two are Vallbona de les Monges and Santes Creus. The kings of Aragón and the noble family members of that time were buried inside the monastery.

2.2. Samples

In Table 1, the labeling, the origin of the samples, the type of bone and the apparent sickness (determined through the macroscopic criteria described in the following lines) are presented. The recognized pathologies were syphilis, osteoporosis and hyperostosis as follows.

In primary syphilis, macroscopic bone changes are very rare; the most important modifications in the skeleton are not found until patients enter the tertiary stage of disease. Lesions are most evident on the frontal bone, they are *caries sicca*, lesions showing erosion, remodeling and scarring all present together in the skull. Otherwise, saber tibia without actual bowing is also a feature of syphilis (Waldron, 2009).

Paleopathological studies of osteoporosis have focused on bone mass (*i.e.* bone quantity) and not so much on bone structure (*i.e.* bone quality) (Mays, 2008; Zimmermann et al., 2011). Remember that bone is formed by hydroxyapatite, which is an ion exchanger that means that it may be loaded with heavy metals; for instance, bone density may vary depending on the environment. Thus, the diagnosis is often based on the presence of established fractures; however, the true prevalence is often underestimated (Waldron, 2009).

Hyperostosis is an excessive growth of bone; for instance hyperostosis *frontalis interna* is a condition in which there is a thickening of the internal table of the frontal bone. The thickening may take several forms. Still, it may be easily recognized (Waldron, 2009).

The samples correspond to skulls or tibias. Two healthy skulls and three samples presenting hyperostosis constitute the group of skulls. In the tibia group there is one healthy sample and four samples with syphilis or hyperostosis, and for the sake of comparison a sample of a tibia with osteoporosis is included, Table 1. All samples are Spanish archeological bones.

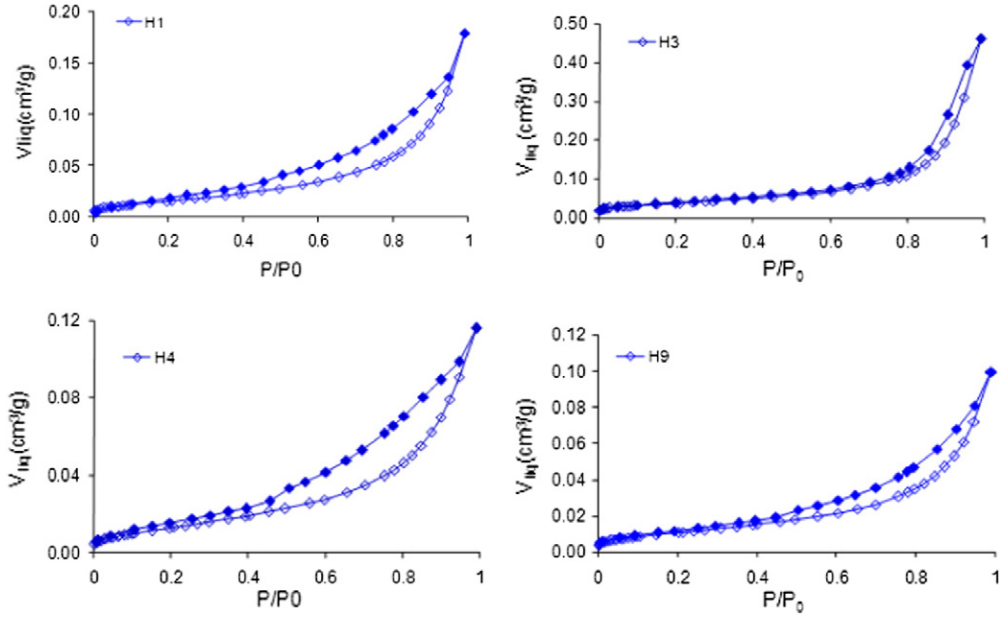

Fig. 2. Nitrogen adsorption isotherms of four Spanish samples obtained at −196 °C; curve H1 corresponds to sample SG-skull-h_1, H3 to sample SG-skull-co, H4 to SG-tibia-h and H9 to SP-tibia-s_1.

Table 2
Surface area and porosity determined by N_2 adsorption isotherms at −196 °C.

Type of bone	Labeling	S_{BET} (m^2/g)	V_P (cm^3/g)	d (nm)
Tibia	SP-tibia-s_1	19	0.10	10.5
	SG-tibia-s_2	64	0.45	14.1
	SG-tibia-hyp	36	0.27	15.0
	SG-tibia-ost	57	0.49	17.2
	SG-tibia-h	24	0.12	10.0
Skull	SG-skull-co	78	0.46	11.8
	SG-skull-hyp_1	65	0.49	15.1
	SG-skull-hyp_2	59	0.34	11.5
	SG-skull-h_1	29	0.18	12.4
	SG-skull-h_2	65	0.41	12.6

2.3. Characterization methods

All samples were studied by nitrogen adsorption–desorption isotherms at −196 °C, SAXS, and SEM. The isotherms were obtained using a Quantachrome automatical equipment with a Quadrasorb. Samples were previously outgassed overnight at 110 °C with a dynamical vacuum of *ca.* 10^{-6} mbar. Adsorption is the adhesion of atoms, ions, or molecules from a gas, a liquid, or a dissolved solid (*i.e.* the adsorbate) to a surface (*i.e.* adsorbent). This process creates a film of the adsorbate on the surface of the adsorbent. For pore structure analysis, the nitrogen adsorption–desorption isotherms were determined. In principle, the nitrogen isotherms of Types II and IV are amenable to the Brunauer–Emmett–Teller (BET) analysis provided that pores of molecular dimensions are absent and that the BET plot is obtained over an appropriate range of the isotherm (Sing, 2001). The BET analysis provides the specific surface area.

SAXS experiments were performed with a Kratky camera. The powdered sample was introduced into a capillary tube. Intensity I(h) was registered as a function of the angular parameter h in $Å^{-1}$, $h = 4\pi\sin\theta/\lambda$, where θ and λ are the scattering angle and the wavelength of the X-rays (a copper X-ray tube was used), respectively. Measurement time was 9 min in order to obtain good quality statistics. The obtained SAXS data were processed with the ITP program (Glatter and Gruber, 1993). The radius of gyration was obtained, as usual, from the slope of the curve Log I(h) *vs* h^2, Guinier plot (Guinier and Fournet, 1955). The globularity of the heterogeneities was estimated from the Kratky plot, *i.e.* $h^2I(h)$ *vs* h. From this plot it is possible to assess if the scattering heterogeneity corresponds to a fibrillar or a globular shape. If the Kratky curve presents a broad peak, the scattering heterogeneities most probably present a globular conformation whereas if the curve approximates a plateau the particles are fibril-like objects (Kataoka et al., 1993, 1994). If the shape is known it is possible to calculate the size distribution functions (Glatter, 1991). SAXS intensity profile contains information about the shape and size of heterogeneities in the material causing a different electronic density, for instance pores between 5 and 25 nm.

SEM studies were performed with a Leica Stereoscan 440 microscope. The samples were previously sputtered with gold to avoid charge problems. Bone morphology revealed by SEM has been often reported (Weiner and Traub, 1992; Weiner and Wagner, 1998). The EDS results correspond to an area of 80 × 70 μm. In the microscope, the elemental identification provided by the EDS probe is very useful. When the sample is homogeneous, one EDS analysis is representative, instead, if the sample is inhomogeneous an EDS analysis of each zone has to be performed. Elements with an atomic weight lower than fluorine are not detected.

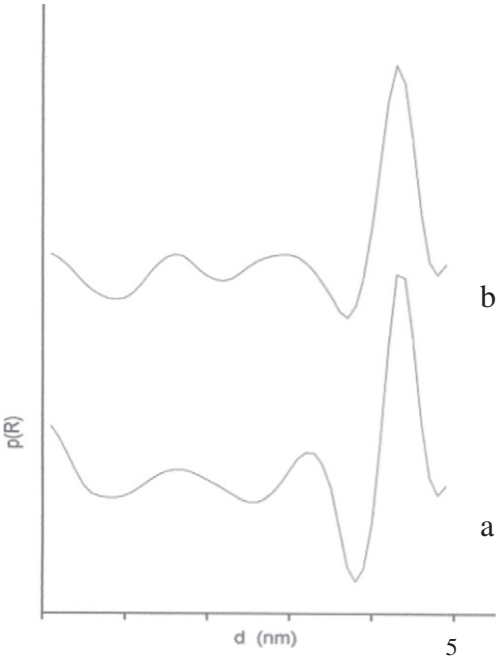

Fig. 3. Heterogeneity size distribution of healthy bones, the differences between the tibia and the skull are minimal: curve a) sample SG-tibia-h; curve b) sample SG-skull-h_2.

3. Results

3.1. Gas adsorption

Fig. 2 shows the adsorption–desorption isotherms at −196 °C obtained on some selected samples as an example. The shape of all isotherms corresponds to the well-known irreversible type II or IIb; they present a hysteresis loop type H3 as defined by IUPAC (Rouquerol et al., 1999). This type of hysteresis loop corresponds to adsorbents constituted by aggregates of platy particles or adsorbents with slit shaped mesopores. It is typical of natural or synthetic hydroxyapatite (El Shafei et al., 2004), clays, and some metal oxides (Rouquerol et al., 1999).

The BET and Dubinin–Radushkevich (DR) equations were applied to the adsorption branch of the isotherms. The BET equation gives the surface area, S_{BET}, and the DR equation the characteristic adsorption energy inside the micropores, which was comprised in all cases

Table 3
Comparison of gyration radii, pore size distributions, and pore shapes determined by SAXS (the underlined values correspond to the highest peak in the distribution).

Type of bone	Labeling	Pore shape	Location of maxima in pore size distribution (nm)	Gyration radius (nm)
Tibia	SP-tibia-s_1	Cylindrical	0.5, 1.8, 3.2	0.460
	SG-tibia-s_2	Cylindrical	0.5, 1.8, 3.2	0.522
	SG-tibia-hyp	Lamellar	1.6, 3.3, 4.4	0.461
	SG-tibia-ost	Cylindrical	0.5, 1.8, 3.2	0.480
	SG-tibia-h	Globular	1.6, 3.3, 4.4	0.520
Skull	SG-skull-co	Cylindrical	0.5, 1.8, 3.2	0.480
	SG-skull-hyp_1	Cylindrical	0.5, 1.8, 3.2	0.581
	SG-skull-hyp_2	Cylindrical	0.5, 1.8, 3.2	0.471
	SG-skull-h_1	Lamellar	1.6, 3.3, 4.4	0.494
	SG-skull-h_2	Globular	1.6, 3.3, 4.4	0.518

Table 4
Morphological features and local composition determined by SEM and EDS.

Type of bone	Labeling	Surface morphology	Ca:P atomic ratio determined by EDS
Tibia	SP-tibia-s_1	Smooth with stones	2.88; 1.65; 1.87
	SG-tibia-s_2	Smoother	1.98; 2.24; 2.04
	SG-tibia-hyp	Stones	1.51; 1.89
	SG-tibia-ost	Stones and feathers	1.67; 1.69
	SG-tibia-h	Smooth with stones	2.00 1.64
Skull	SG-skull-co	Stones and honey comb	1.82; 1.52
	SG-skull-hyp_1	Stones and feathers, typical of bone	2.22; 1.62; 1.89; 2.13
	SG-skull-hyp_2	Smooth, stones and needles	2.13; 2.88; 2.34; 1.74
	SG-skull-h_1	Smooth with cracks	1.66; 1.80
	SG-skull-h_2	Typical bone morphology; large pores	1.71; 2.08

between 11 and 16 kJ/mol. Thus, the samples are not microporous (pores less than 2 nm) as far as this technique is concerned. The total pore volume, V_p, was obtained from the amount of (liquid) nitrogen adsorbed at a relative pressure $p/p_0 = 1$. If mesopores are slit-like, their mean width, d, may be estimated using the equation $d = 2V_p/S_{BET}$. The resulting values of S_{BET}, V_p and d are compiled in Table 2.

The surface area values of the healthy bones (SG-tibia-h; SG-skull-h_1) are between 24 and 29 m^2/g and the mean width of their slit-like pores is *ca.* 11.2 nm. This value corresponds to the size of canaliculi, more precisely to periosteocytic space. The sick bones present a specific surface area between 36 and 78 m^2/g. The value obtained for sample SG-skull-h_2 (i.e., 65 m^2/g) is too high. This result will be discussed later on, as well as the value obtained for the Poblet tibia (19 m^2/g), which is out of all expectations.

3.2. Small angle X-ray scattering

The shape of heterogeneities, the diameters corresponding to the peaks of the pore size distributions, and the gyration radii are compared in Table 3. The healthy samples SG-skull-h_1, SG-skull-h_2, and SG-tibia-h are characterized by the same heterogeneity size distributions with a main peak for a diameter of 4.4 nm, Fig. 3, the gyration radii of these bones are 0.494, 0.518 and 0.520 nm respectively. The two samples with the same gyration radius have similar heterogeneity shape (globular), while in sample SG-skull-h_1 pores are slit shaped. Note that SAXS is a "bulk" method, *i.e.* the measurements correspond to the volume of the sample and not to the accessible surface as in gas adsorption. Bubbles, as well as encapsulated pores, are detected by SAXS and not by gas adsorption. Furthermore, as SAXS is due to differences in the electron density it corresponds to pores (lower electron density than the average) as well as dense particles or agglomerates (higher electron density than the average). Pores and dense particles are heterogeneities present in the material.

Most probably, the peaks at *ca.* 4.0 nm correspond to the microfibril diameter. In healthy bones it is 4.4 nm, whereas in sick bones it is 3.2 nm. Only, the sick bone SG-tibia-hyp seems to reproduce the "healthy" values. Those fibrils are known to be constituted by aggregates of tropocollagen whose length is *ca.* 300 nm and whose diameter is 1.5 nm. Therefore the peaks at 1.8 nm should correspond to tropocollagen diameter. It is observed in healthy (1.6 nm) and sick bones (1.8 nm), showing that, in these bones, tropocollagen molecules are slightly swelled.

Still, this point illustrates the difficulty of interpretation of SAXS measurements in systems as complex as bone. Again, SAXS is due to electron density contrast among hydroxyapatite particles, collagen or pores, and the surrounding medium. The SAXS curve is mostly due to the highest contrast, which in this case, is the electron density contrast between the mineral and collagenous components. However, when a microporosity, due to sickness or diagenesis, arises, the interpretation may not be clear.

Gyration or Guinier radii are a useful estimate of size, as no need of assumed shape is required to calculate it. The gyration radii of sphere or needle shaped heterogeneities may be compared. It is the root mean square distance of the object´s parts from either its center of gravity or a given axis.

3.3. Scanning electron microscopy

As it is not possible to show all micrographs, their main features are described in Table 4, "stones" mean that there are large particles on the surface which may be "smooth" or "rough". The small rod-like mineral crystallites in fresh human bone are designed, here, as "feather-like"; they are typical of bone surfaces and they are often observed in healthy bones, Fig. 4 (Weiner and Traub, 1992; Pijoan et al., 2007).

The three healthy bones present a local atomic Ca:P ratio comprised between 1.64 and 2.08. Still, SG-skull-h_2 atomic Ca:P is higher, *i.e.* the bone has lost phosphates, and large pores are apparent in the micrographs. The other two healthy bones are smoother and present large particles on the surface.

The three samples with hyperostosis are very heterogeneous, for instance, the Ca:P atomic ratio in sample SG-skull-hyp_2 varies from 1.74 to 2.88 depending on analysis location. If SG-tibia-hyp, SG-skull-hyp_1 and SG-skull-hyp_2 are compared the Ca:P ratio varies from Ca:P = 1.51 to

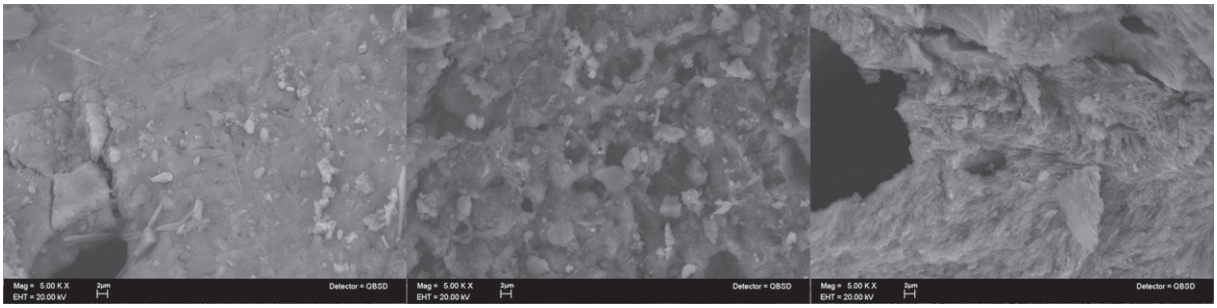

a) b) c)

Fig. 4. Typical morphologies observed by SEM: a) smooth (sample SG-tibia-s_2), b) stones (SG-tibia-h), and c) featherlike (SG-skull-h_2).

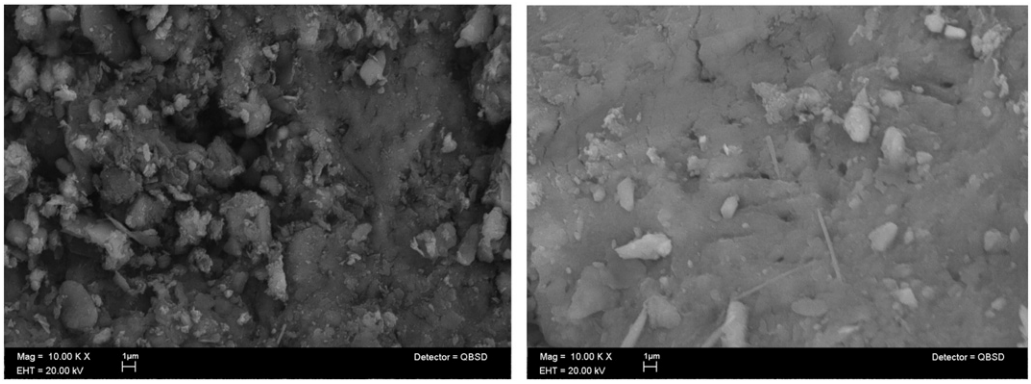

Fig. 5. SEM images, at 10,000 magnification, of SP-tibia-s_1 (left hand side) and SG-tibia-s_2 (right hand side). They both correspond to syphilitic bones and their morphology is rather similar (smooth with stones).

2.88. The morphology is characterized by stone presence on a rather smooth surface.

Such is not the case for the osteoporotic sample (SG-tibia-ost) where the Ca:P atomic ratio seems to be constant all over and equal to 1.67–1.69 which corresponds to the value found for healthy bones. Furthermore the value reported for human bones is 1.66 (Miculescu et al., 2011). Again, stones are observed, but the surface is no longer smooth. The sample with *criba orbitalia* (SG-skull-co) reproduces this morphology although the Ca:P atomic ratio is rather heterogeneous (1.52 to 1.82).

Although they differ in their origin (Poblet and Granada), syphilitic tibia samples (SP-tibia-s_1 and SG-tibia-s_2) present a similar smooth surface with different degrees of deterioration, Fig. 5.

4. Discussion

The porous system of bone is hierarchical, two size ranges may be distinguished; on the one hand, a micrometric porosity (Haver) and, on the other, a less than a micron one (lacunae, a few μm, and canaliculi, less than 1 μm). It has to be emphasized that cells, water and fluids occupy the fresh bone porous system and, thus, archeological bone may contain their residues. The various characterization techniques were chosen as they are complementary, SAXS is adequate to study microporous heterogeneities, gas adsorption is sensible to open and accessible micropores and mesopores, and scanning electron microscopy is efficient at the micron range. Some of our results, as already stated, may seem contradictory.

The obtained values of specific surface area for healthy bones (29 and 11 m^2/g) are more than twice those reported by ourselves for boiled human bones, all comprising between 2 and 7 m^2/g (Bosch et al., 2011). Such difference may be explained if sample pretreatment is considered. In our previous work, the samples were outgassed *in vacuo* at 80 °C. In the present one, they were treated overnight at 110 °C with a dynamical vacuum of *ca.* 10^{-6} mbar. This point is crucial to compare results. Depending on pretreatment method (degasification method, liophilization, or treatment with solvents), specific surface areas between 0.19 m^2/g and 101 m^2/g, in modern and old bovine bones, were obtained by Smith et al. (2008).

It remains to be explained why the specific surface area of SG-skull-h_2, which is a healthy sample, corresponds to the values obtained for sick materials. Most probably it is because the bone sample is, indeed, a sick bone and the macroscopical criterion has failed. SEM found large pores, not present in the other healthy samples. The ratio Ca:P (1.71 and 2.08) reveals that the composition is rather inhomogeneous. Instead, SAXS results agree with those obtained for other healthy bones. It seems then that, at micro-level, the sample corresponds to a healthy material; but at mesoporous level it is a sick sample. This difference fits with the conclusions of Wang and Ni (2003) and Martin (1984) who have shown that, in osteoporotic bones, Harvesian canals (large pores) increase significantly with age whereas lacuna porosity decreases slightly.

Sample SG-tibia-hyp can be understood if various degrees of sickness, *i.e.* of growing porosity, are accepted. The macroscopical approach is qualitative while the micrometrical focus may be quantitative in the sense that the progression of sickness may be determined. Although, those variations could be attributed, as well, to different pore obstructions due to the environment, or to residues occluded in cavities. Water has to be discarded as the samples were treated overnight at 110 °C *in vacuo*. The peaks of SG-tibia-hyp, in the SAXS size distribution, are located at 1.6, 3.3 and 4.4 nm as in a healthy bone. Hence, this bone is not "so sick".

These concepts are well illustrated by the SEM micrographs of Fig. 5, which correspond to syphilitic bones. A rather smooth surface is observed in the SG-tibia-s_2, which is reproduced by sample SP-tibia-s_1 but with more "stones". It seems then that the morphology of syphilitic bone is the same independent of the provenance or other alterations such as age or *postmortem* environment.

5. Conclusion

Porosity may be differentiated at a micrometrical level using techniques such as scanning electron microscopy, small angle X-ray scattering, or gas adsorption. Measurements are very sensitive to cleaning and thermal treatments. Even if macroscopically bones may be classified as healthy, osteoporotic, hyperostosic or syphilitic, the micrometrical characterization shows that there is a broad range where the bone may be "partially" sick. This conclusion is important as some pathology may attack selectively a range of pore sizes (micropores, for instance) and not others. Diagenesis processes may result in similar morphologies as those produced by pathologies (Aufderheide, 2011); thus, the context and history of samples has to be well known.

Last but not least, the study of bone porosity is hard work and it cannot be described with a sole technique. To distinguish if the porosity of a bone corresponds to a healthy one or not, complementary characterization methods, at least those used in this work, have to be utilized. Indeed, SAXS is due to close and open micropores, N_2 adsorption is related to micro and mesopores which must be open and accessible to nitrogen molecules at the adsorption temperature, and SEM provides local information on surface morphology (macropores).

Acknowledgments

The technical work in electron scanning microscopy of Omar Novelo is gratefully acknowledged. I. Leboreiro took the bone samples. His work was essential for this study.

References

Aufderheide, A.C., 2011. Soft tissue taphonomy: a paleopathology perspective. Int. J. Paleopathol. 1, 75–80.

Barrère, F., van Blitterswijk, C.A., de Groot, K., 2006. Bone regeneration: molecular and cellular interactions with calcium phosphate ceramics. Int. J. Nanomedicine 1, 317–332.

Bosch, P., Alemán, I., Moreno-Castilla, C., Botella, M., 2011. Boiled versus unboiled: a study on Neolithic and contemporary human bones. J. Archaeol. Sci. 38, 2561–2570.

Domínguez-Rodrigo, M., Pickering, T.R., Diez-Martín, F., Mabulla, A., Musiba, C., Trancho, G., Baquedano, E., Bunn, H.T., Barboni, D., Santonja, M., Uribelarrea, D., Ashley, G.M., Martínez-Ávila Ma. del, S., Barba, R., Gidna, A., Yravedra, J., Arriaza, C., 2012. Earliest porotic hyperostosis on a 1.5-million-year-old Hominin, Olduvai Gorge, Tanzania. PLoS ONE 7, e46414. http://dx.doi.org/10.1371/journal.pone.0046414.

El Shafei, G.M., Philip, C.A., Moussa, N.A., 2004. Fractal analysis of hydroxyapatite from nitrogen isotherms. J. Colloid Interface Sci. 277, 410–416.

Fairén-Jiménez, D., Carrasco-Marín, F., Djurado, D., Bley, F., Ehrburger-Dolle, F., Moreno-Castilla, C., 2006. Surface area and microporosity of carbon aerogels from gas adsorption and small- and wide-angle X-ray scattering measurements. J. Phys. Chem. B 110, 8681–8688.

Glatter, O., 1991. Scattering studies on colloids of biological interest. Progr. Colloid Polym. Sci. 84, 46–54.

Glatter, O., Gruber, K., 1993. Indirect transformation in reciprocal space: desmearing of small-angle scattering data from partially ordered systems. J. Appl. Crystallogr. 26, 512–518.

Guinier, A., Fournet, G., 1955. Small Angle Scattering of X-rays. Wiley, New York.

Hiller, J.C., Wess, T.J., 2006. The use of small-angle X-ray scattering to study archaeological and experimentally altered bone. J. Archaeol. Sci. 33, 560–572.

Kataoka, M., Hagihara, Y., Mihara, K., Goto, Y., 1993. Molten globules of cytocrome c studied by the small angle X-ray scattering. J. Mol. Biol. 229, 591–596.

Kataoka, M., Flanagan, J.M., Tokunaga, F., Engelman, D.M., 1994. Use of X-ray solution scattering for protein folding study in synchrotron radiation. In: Chanse, B., Deisenhofer, J., Ebashi, S., Goodhead, D.T., Huxley, H.E. (Eds.), The Biosciences 4. Clarendon Press, Oxford, U.K., pp. 87–92.

Labastida Pólito, A., Piña Barba, C., Tello Solís, S., 2006. Collagen type I scaffolds for use in medicine. AIP Conf. Proc. 854, 129–131.

Lopes, C., Powell, M.L., Santos, A.L., 2010. Syphilis and cirrhosis: a lethal combination in a XIX century individual identified from the medical schools collection at the University of Coimbra (Portugal). Mem. Inst. Oswaldo Cruz, Rio de Janeiro 105, 1050–1053.

Martin, R.B., 1984. Porosity and Specific Surface of Bone, CRC Critical Reviews in Biomedical Engineering, Boca Raton, FL ,pp. 179–222.

Mays, S., 2008. Metabolic bone disease. In: Pinhasi, R., Mays, S. (Eds.), Advances in Human Palaeopathology. John Wiley & Sons, West Sussex, UK, pp. 214–251.

Miculescu, F., Ciocan, L.T., Miculescu, M., Ernuteanu, A., 2011. Effect of heating process on micro structure level of cortical bone prepared for compositional analysis. Dig. J. Nanomater. Bios. 6, 225–233.

Ortner, D.J., 2011. Human skeletal paleopathology. Int. J. Paleopathol. 1, 4–11.

Pijoan, C.Ma., Mansilla, J., Leboreiro, I., Lara, V.H., Bosch, P., 2007. Thermal alterations in archaeological bones. Archaeometry 49, 713–727.

Roffey, S., Tucker, K., 2012. A contextual study of the medieval hospital and cemetery of St Mary Magdalen, Winchester, England. Int. J. Paleopathol. 2, 170–180.

Rouquerol, J., Rouquerol, F., Sing, K.S.W., 1999. Adsorption by Powders and Porous Solids: Principles, Methodology and Applications. Academic Press, San Diego, USA.

Sing, K., 2001. The use of nitrogen adsorption for the characterization of porous materials. Colloids Surf. A Physicochem. Eng. Asp. 187–188, 3–9.

Smith, C.I., Faraldos, M., Fernández-Jalvo, Y., 2008. The precision of porosity measurements: effects of sample pre-treatment on porosity measurements of modern and archaeological bone. Palaeogeogr. Palaeoclimatol. Palaeoecol. 266, 175–182.

Waldron, T., 2009. Palaeopathology. Manuals in Archaeology. Cambridge University Press, Cambridge.

Walker, P.L., Bathurst, R.R., Richman, R., Gjerdrum, T., Andrushko, V.A., 2009. The causes of porotic hyperostosis and criba orbitalia: a reappraisal of the iron-deficiency-anemia hypothesis. Am. J. Phys. Anthropol. 139, 109–125.

Wang, X., Ni, Q., 2003. Determination of cortical bone porosity and pore size distribution using a low field pulsed NMR approach. J. Orthop. Res. 21, 312–319.

Weiner, S., Traub, W., 1992. Bone structure: from ångstroms to microns. FASEB J. 6, 879–885.

Weiner, S., Wagner, H., 1998. The material bone: structure–mechanical function relations. Annu. Rev. Mater. Sci. 28, 271–298.

Zimmermann, E.A., Schaible, E., Bale, H., Barth, H.D., Tang, S.Y., Reichert, P., Busse, B., Alliston, T., Ager III, J.W., Ritchie, R.O., 2011. Age-related changes in the plasticity and toughness of human cortical bone at multiple length scales. PNAS 108, 14416–14421.